

Two-dimensional and Three-dimensional Moving Finite Element Analysis for High-speed Crack Propagation in Brittle Materials

T. Nishioka¹, K. Yamaguchi¹, H. Furuta¹, T. Fujimoto¹

Summary

Based on experimental results, in this study, two and three dimensional generation-phase simulations for these high-speed crack propagation phenomena are carried out. The numerical simulations results provided energy flow to crack tip, the relationship of 3-D crack surface roughness versus the Φ_{total} parameters and the distributions of the dynamic J integral along the crack front.

Introduction

There have been several studies on limiting crack velocities in an elastic homogeneous material. According to energy theory of dynamic fracture mechanics, the crack propagation velocity C cannot exceed the Rayleigh wave velocity C_R . Moreover, considering only the stress singular term near the crack tip, the analytical asymptotic stress field, suggests the maximum hoop stress deviates from the crack propagation direction when the crack velocity exceeds 60% of the shear wave velocity ($C > 0.6C_s$) [1]. Therefore, until recently it has been considered that the straight crack propagation exceeding $0.6C_s$ never occurs.

However, in the latest research, straight crack progress exceeding $0.6C_s$ is observed by experiment in the high-speed crack propagation in a fracture test and an Interface crack, in which the load system was pluralized. Therefore, it is necessary to reconsider the mechanism which defines the limit of crack propagation velocity.

In our previous experimental study [2], the cracks were critically accelerated by using a multi-loading system. One of the crack propagation velocities reached 74% of the shear wave velocity. From the experimental study, loading histories, crack propagation histories and C.G.S. fringes were obtained.

Based on these experimental results, in this study, two and three dimensional generation-phase simulations for these high-speed crack propagation phenomena are carried out. The generation-phase simulations are performed to estimate fracture energy flow and other parameters. Energy flow to crack tip are visualized by 2-D numerical simulation. In 3-D numerical simulation, the relationship of 3-D crack surface roughness and Φ_{total} parameters are obtained. The increase of the dynamic J integral with the increase of crack propagation velocity is measured in numerical simulations. Furthermore, the distributions of the dynamic J integral along the crack front are obtained.

¹ Faculty of Maritime Sciences, Kobe University, Kobe, Japan

Measurement of the Dynamic J Integral using the Equivalent Domain Integral (EDI) Method

In this study, one of the fracture mechanics parameters, the dynamic J integral, as defined by Nishioka and Atluri [3], is used. The dynamic J integral is very attractive due to the following reasons: It has the physical meaning of the dynamic energy release rate; It has the property of being a path-independent integral; It can be related to the dynamic stress intensity factors by shrinking the integral path to the crack tip.

In order to evaluate fracture parameters along a three-dimensional crack front, Nishioka et al [4], developed the following procedures using the dynamic J integral [3]:

$$J_k = \lim_{\Gamma_\epsilon \rightarrow 0} \int_{\Gamma_\epsilon} [(W+K)n_k-t_i u_{i,k}] dS \tag{1}$$

$$= \lim_{\Gamma_\epsilon \rightarrow 0} \left(\int_{\Gamma+\Gamma_c} [(W+K)n_k-t_i u_{i,k}] dS + \int_{V_\Gamma-V_\epsilon} [\rho \ddot{u}_i u_{i,k} - \rho \dot{u}_i \dot{u}_{i,k}] dV \right) \tag{2}$$

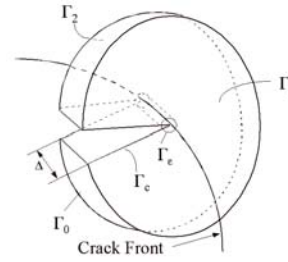


Fig.1 Crack front segment

where W and K are the strain and kinetic energy density, respectively; n_k are the outward normal-direction cosines; t_i is the traction; u_i , \dot{u}_i , and \ddot{u}_i are the components of displacement, velocity and acceleration of a material point, respectively; ρ is mass density; Γ_ϵ is a near-field contour arbitrary close to the propagating crack-tip; Γ is an arbitrary far-field path; V_Γ and V_ϵ are the volumes enclosed by $\Gamma+\Gamma_c$ and Γ_ϵ , respectively.

In order to ease the three-dimensional numerical evaluation of the dynamic J integral, an expression of dynamic J integral terms of equivalent domain integral (EDI) was developed [5]. Suppose that the crack front is divided into segments (see Fig.1), using a continuous function s that takes a non-zero value on the near-field path and the far-field paths, then the following equivalent domain integral expression is derived:

$$J_k = \frac{1}{f} \left(\int_{V_\Gamma} [\sigma_{ij} u_{i,k} s_{,j} - (W+K) s_{,k} + (\rho \ddot{u}_i u_{i,k} - \rho \dot{u}_i \dot{u}_{i,k}) s] dV + \int_{\Gamma_1+\Gamma_2} [(W+K)n_k-t_i u_{i,k}] s dS \right) \tag{3}$$

In this study, we use two types of s functions [6] as presented in Fig.2. Type A gives the value of the dynamic J at the central corner node, and type C gives the value of the dynamic J at the mid-node, in a sense of a weighted mean. To evaluate the dynamic J integral at all nodes along the crack front, both types of the s function are jointly used.

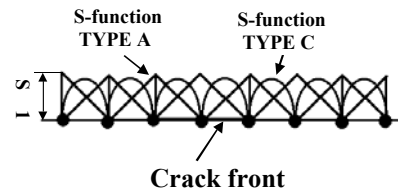


Fig.2 Typical s function

The s function can be interpolated using the shape functions of the 20-noded isoparametric elements, which are also used for the displacement field:

$$s = \sum_{q=1}^{20} N_q(\xi, \eta, \zeta) s_q \quad (4)$$

where N_q and s_q are the shape function and the value of the s function at the node q , respectively.

Substituting Eq. (5) into Eq. (4), the dynamic J integral can be evaluated by:

$$J'_k = \sum_{n=1}^{N_v} \sum_{q=1}^{20} R_{knq} s_q + \sum_{n=1}^{N_s} \sum_{q=1}^{20} Q_{knq} s_q \quad (5)$$

$$R_{knq} = \int_{V_n} [\sigma_{ij} u_{i,k} N_{q,j} - (W+K) N_{q,k} + (\rho \dot{u}_i u_{i,k} - \rho \dot{u}_i u_{i,k}) N_q] dV \quad (6)$$

$$Q_{knq} = \int_{S_n} [(W+K) n_k - t_i u_{i,k}] N_q dS \quad (7)$$

in which f is the integral value of s function along a segment of crack-front under consideration; N_v and N_s are the total number of elements in V_r and on the $\Gamma_1 + \Gamma_2$; V_n and S_n are the volume and surface on the n -th element, respectively.

Using the nature of the dynamic J as a vector, to avoid using transformation for stress and strain and other fields at all integration points in V_r , the local components of dynamic J integral can be determined from the global components of the dynamic J integral through the relation

$$J^0_l = \alpha_{lk} J'_k \quad (8)$$

where α_{lk} is the coordinate transformation tensor from the global coordinates $X_k (k=1,2,3)$ to the crack-front coordinates $x_l^0 (l=1,2,3)$.

Three-Dimensional Moving Finite Element Method [7]

In the moving finite element method, three-dimensional 20-noded isoparametric elements are used. The 20-noded isoparametric elements used in the mesh are divided into three types: Type A: moving elements, Type B: distorting elements, Type C: non-distorting elements, respectively. Type A elements near the crack front translate in each time step for which crack growth occurs. Type B elements, surrounding the moving elements are continuously distorted.

The mesh pattern for the elements near the crack-tip translates in each time step for which the crack growth occurs. Thus, the crack-tip always remains at the center of the moving elements throughout the analysis. In order to simulate a large amount of crack propagation, the mesh pattern around the moving elements is periodically readjusted.

For the time integration of equation of motion, the Newmark β method is used. To obtain the numerical solution at the current steps, the nodal displacements, velocities and accelerations at the previous step are required. Therefore, the displacements, velocities and accelerations at the newly created nodes after shifting or readjusting the mesh pattern are required to obtain the interpolation of the field of variables at the old nodes.

Numerical results

The basic geometry configuration under consideration is presented in Fig.3. The specimen was made of PMMA (polymethyl methacrylate) with the material properties of Young's modulus $E=2.948$ GPa, Poisson's ratio $\nu=0.329$ and Mass density $\rho=1190$ kg/m³. The dilatation, shear and Rayleigh wave velocities in the material are $C_d=1666.7$, $C_s=965.4$ and $C_R=898.6$ m/sec, respectively.

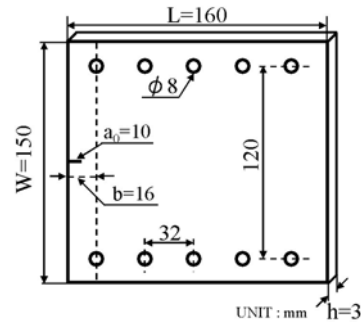


Fig. 3 Specimen geometry

Using the experimentally recorded loading histories and crack propagation histories, the generation-phase simulation were carried out. The loading histories in each pin are shown in Fig.4. The load was applied as an equivalent nodal force through the specimen thickness. Furthermore, the crack propagation history and crack velocity history are summarized in Fig.5. By assuming the shape of the crack-front to be linear, the generation-phase simulation was carried out.

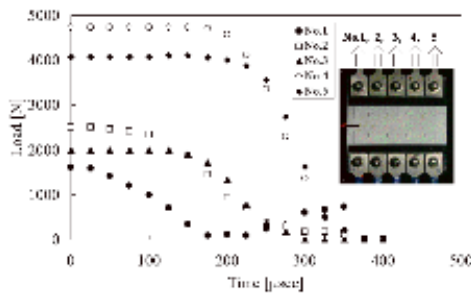


Fig.4 Load values history

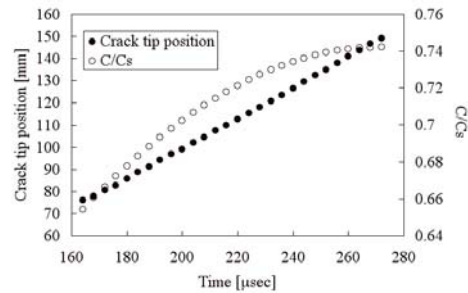


Fig.5 Crack propagation and crack velocity histories

In two-dimensional numerical simulation, by the moving finite element method based on Delaunay automatic triangulation, the generation-phase simulation was carried out. The mesh consists of 9660 elements and 5000 nodes. For the numerical simulation the time increment of 0.25 μ sec is used.

Due to the symmetry of the geometry and the loading condition, in the three-dimensional numerical simulation, only the upper part of the specimens was modeled in

the analysis. Six layers of 20-noded isoparametric moving elements through the thickness were used. The mesh consists of 3252 elements and 15767 nodes. For the numerical simulation the time increment of 0.25 μ sec is used.

The dynamic J integral histories for two-dimensional problems and for three-dimensional problems at the surface ($Z=0$) and mid-plane ($Z=1/2h$) of the plate are shown in Fig.6. At this time, for each far-field path, excellent path independence was obtained. It can be observed from Fig.6 that the dynamic J integral values increases with the increases of the crack propagation velocity. However, the dynamic J integral decreases rapidly after $C/C_s=0.74$. Also, the dynamic J integral value of the mid-plane ($Z=1/2h$) takes the value which is higher than the dynamic J integral value of the surface ($Z=0$). The difference increases with the increase in the crack propagation velocity.

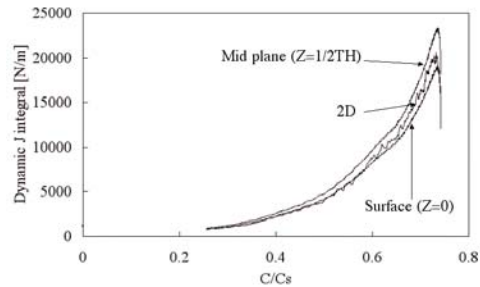


Fig.6 Dynamic J integral histories

The distributions of the dynamic J integral along the crack-fronts are shown in Fig.7. At the crack tip on each layer, the constant dynamic J integral values have been obtained under $C/C_s < 0.53$. Thus, the dynamic fracture event is done in two-dimensional deformation and destruction condition under this crack propagation velocity. However, it is seen that the dynamic J integral takes the maximum values at mid-plane of the plate when the crack propagation velocity reaches $C/C_s > 0.7$.

Fig.8 shows the relationship between the crack surface roughness at surface ($Z=0$), quarter-plane ($Z=1/4h$) and mid-plane ($Z=1/2h$) of the plate measured by experimental results, and the parameter Φ_{total} , which means the energy inflow per unit time to crack surface obtained by three-dimensional numerical simulation. The Φ_{total} is calculated based on the crack propagation velocity C and the dynamic J integral J_I^0 . It is seen that the value of Φ_{total} increases when the crack surface roughness increases. In addition, in the surface

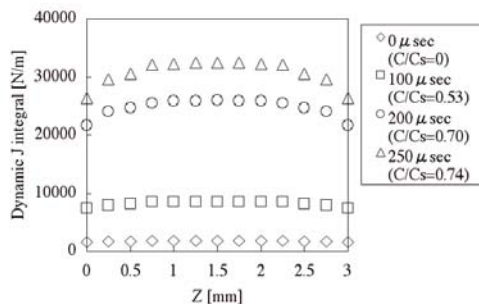


Fig.7 Distribution of dynamic J integral

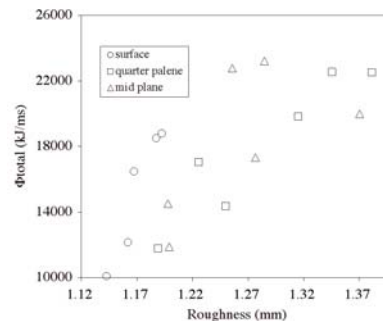


Fig.8 Relation between crack surface roughness and Φ_{total}

($Z=0$), both the crack surface roughness and the Φ_{total} take on a low value compared with the values at the quarter-plane ($Z=1/4h$), mid-plane ($Z=1/2h$) of the plate.

Conclusions

In this study, based on experimentally recorded history of high-speed crack propagation phenomena, two and three dimensional generation-phase simulations were carried out. From the numerical results, behaviors of the dynamic J integral during high-speed crack propagation were clarified. Moreover, it was found that with the increase in the crack propagation velocity, the fracture mechanics parameter at the crack tip on each layer was not constant. It was also seen that the change of the dynamic J integral values depend on the energy flow into the crack tip. Finally, the relations between the experimental crack surface roughness and Φ_{total} were measured.

Acknowledgement

This study was supported by the Grant-in-Aid for Scientific Research (NO.14205019) from the Japan Society for Promotion of Science.

Reference

- 1 Yoffe, E. H. (1951): "The moving Griffith crack", *Philosophical Magazine*, Vol. 42, pp. 739-750.
- 2 Nishioka, T., Sakaguchi, Y., Fujimoto, T. and Sakakura, K. (2003): "Experimental Study on Limiting Fracture Velocities in Homogeneous Materials", Symposium on Recent Advances in Dynamic Failure and Fracture Studies, The 2003 Society for Experimental Mechanics Annual Conference.
- 3 Nishioka, T. and Atluri, S. N. (1983): "Path Independent Integrals, Energy Release Rates and General Solutions of Near-Tip Fields in Mixed-Mode Dynamic Fracture Mechanics", *Eng. Fract. Mech.*, Vol. 18, pp. 1-22.
- 4 Nishioka, T., Yoshimura, S., Nishi, M. and Sakakura, K. (1995): "Experimental Study on Three-Dimensional Dynamic Fracture", *Dynamic Fracture, Failure and Deformation*, (T. Nishioka and J.S. Epstein. Eds.), ASEM Publ. Pvp-300, pp. 87-97.
- 5 Nishioka, T., Ichikawa, Y. and Maeda, N. (1995): "Numerical Study on Three-Dimensional Dynamic Fracture", *Dynamic Fracture, Failure and Deformation*, (T. Nishioka and J.S. Epstein. Eds.), ASEM Publ. Pvp-300, pp. 73-85.
- 6 Nikishkov, G. P. and Atluri, S. N. (1987): "Calculation of Fracture Mechanics Parameter for an Arbitrary Three-Dimensional Crack, by the Equivalent Domain Integral", *Int. J. Num. Methods in Eng.*, Vol. 24, pp. 1801-1821.
- 7 Nishioka, T., Stan, F. and Fujimoto, T. (2002): "Dynamic J Integral and Dynamic Stress Intensity Factor Distributions along Naturally and Dynamic Propagating Three-Dimensional Fracture Fronts", *JSME International Journal, Series A*, Vol. 45, No. 4, pp. 523-537.